Assessment of fatigue load alleviation potential through blade trailing edge morphing

2016 J. Phys.: Conf. Ser. 753 042020

(http://iopscience.iop.org/1742-6596/753/4/042020)

Assessment of fatigue load alleviation potential through blade trailing edge morphing

Theofanis Tsiantas[1], Dimitris I. Manolas[1], Theodore Machairas[2], Anargyros Karakalas[2], Vasilis A. Riziotis[1], Dimitrios Saravanos[2], Spyros G. Voutsinas[1]

[1]School of Mechanical Engineering, National Technical University of Athens, GR15780 Athens, Greece
[2]Department of Mechanical Engineering and Aeronautics, University of Patras, Patras, Greece

Correspondance to: vasilis@fluid.mech.ntua.gr

Abstract. The possibility of alleviating wind turbine loads through blade trailing edge shape morphing is investigated in the present paper. Emphasis is put on analyzing the effect of the trailing edge flap geometry on load reduction levels. The choice of the shape deformation of the camber line as well as the chordwise and spanwise dimensions of the trailing edge flap are addressed. The analysis concerns the conceptual DTU 10 MW RWT. Aeroelastic control of loads is materialized through a standard individual flap controller. Furthermore, a combined individual pitch-flap controller is evaluated and found to present advantages compared to the flap only controller. Flapwise fatigue load reduction ranging from 10% to 20%, depending on wind velocity and configuration considered, is obtained. Better performance is achieved by the combined pitch-flap controller.

1. Introduction

The possibility of alleviating wind turbine blade loads by means of trailing edge (TE) shape morphing techniques is investigated in the framework of Work Package 2 of the INNWIND.EU project. Load alleviation is realized through active control of the camber line shape in the TE area. The development of blade sections capable of undergoing significant geometry adaptations to optimally and timely respond to wind fluctuations is the key objective for successful control of loads. Ongoing research conducted by the University of Patras (UP) and the National Technical University of Athens (NTUA) is focused on designing Shape Memory Alloy (SMA) actuators as a mean for active load control. It has been shown in [1] and [2] that SMA actuators can constitute the basis for effectively controlling the shape of the blade camber line when implemented along with an appropriate morphing mechanism. The present study is mainly focusing on the definition of the appropriate morphing shape and the required chordwise and spanwise extent of the TE flap, so that satisfactory fatigue load reduction is achieved with control actuation speeds attainable by SMA type actuators.

Aeroelastic control of the blade fatigue loads is realized through the use of a standard individual flap controller (IFC). The controller is based on the decomposition of the blade root out-of-plane moments of the three blades (measured in the rotating reference frame) into yaw and tilt moments in the hub fixed system (expressed in the non-rotating frame) through application of Coleman's transformation. The hub fixed moments represent the control input variables through which two output cyclic flap angles are defined. Re-modulation of the output cyclic flap angles by means of the inverse Coleman transformation provides the individual flap angles of the three blades [3]. Furthermore a

combined individual pitch-flap control (IPFC) is tested based on the same working principle. In the IPFC controller, individual flap control is augmented by simultaneous individual control of the pitch angle of the three blades.

The smooth output of IFC and IPFC controllers that follows a 1p variation, seems to be well suited for the relatively slow SMA actuators (as compared to conventional ones), especially for slowly rotating large rotors. In this work, Shape Memory Alloy in 1D form (wires) are considered, in order to provide the actuation forces required to morph the flap to the desired configuration. Due to their intrinsic high actuation energy density they are adequate for lightweight morphing concepts and large movements. Preliminary studies presented in [1], [2] have proven that SMA's can perform satisfactorily at 1p actuation frequencies. Therefore, they are adopted as actuators in this study, instead of conventional actuators, such as servomotors or pneumatic actuators, due to their simplicity, compactness and performance. An articulated finger like mechanism has been designed as baseline actuator. This morphing mechanism is activated by pairs of SMA wire actuators in an antagonistic configuration scheme.

Higher load reduction requirements on larger rotor can be met by extending the length of the TE flap in the chordwise direction. As discussed next, the requirement for longer flaps that undergo large curvature variations can be satisfied through the use of multi-element sections in which multiple SMA wires can be easily accommodated, as shown in [1], [2]. In the present work the effect of different morphing shapes of the TE region on the lift characteristics of the blade section is assessed. Once the appropriate trailing edge shape is fixed, load reduction capabilities are assessed for different chordwise and spanwise lengths of the control surface.

It is noted that both IFC and IPFC methods have been tested by several researchers in the past years. Most recent developments are those of Lackner and van Kuik [4], Bæk [5] and Bernhammer et al [6] who have all applied similar IFC and IPFC schemes based on Coleman's transformation in order to reduce blade fatigue loads. Also, of relevance are the works by Barlas et al [7] and Bergami and Poulsen [8] who have applied model predictive and linear quadratic control of adaptive distributed flap geometries. The novelty of the present analysis consists of considering the DTU Reference Innwind.eu 10 MW (D=178.3 m) wind turbine (RWT) [9], while all previous developments concerned the NREL 5 MW turbine. As reported in [10], the increase in rotor diameter lowers the rotational frequency, which then gets closer to the frequency range that the wind spectrum has its maximum energy. Thereby, the rotational sampling of the wind turbulence by the rotating blades will concentrate more of the total turbulence spectrum energy on low p multiples. As a result, 1p variation of loads is expected to be higher for larger rotors and therefore more demanding requirements are set on the active load alleviation devices.

In the field of SMAs, the development of the technology has reached a quite high level and a variety of commercial solutions is available. Modeling and implementation of novel numerical tools [11], [12] provide the background for designing morphing devices driven by these materials. Although the main field for such applications is aerospace technology [13], wind turbine technology tends to adopt these materials for structural morphing as a load alleviation technique [14], [15]. In order for load alleviation to be achieved the SMA actuators need to follow target time trajectories by undergoing transformation strain. The response of the actuators is highly driven by the heating/cooling rate [16] provided and this is a limitation for their usage.

The present work is mainly focusing on fatigue load reduction capabilities of trailing edge morphing controllers. However, the effect on blade extreme loads is also checked. A reduction of the flapwise fatigue moment at the root of the blade ranging from about 10% to 20% is obtained, depending on the wind velocity and the configuration considered. Overall the tower fatigue loads slightly increase while extreme flapwise loads slightly decrease. The rate is again very much dependent on the configuration. Finally the effect of the flap controller operation on the output power is found negligible especially in the full load region.

2. Description of the aeroelastic tool

Load reduction capabilities are assessed through simulations using the state of the art servo-aero-elastic solver hGAST [17], [18],[19]. In hGAST the full wind turbine is considered as a multi-component dynamic system having as components the blades, the drive train and the tower; all components are approximated as beam structures. Assembly into the full system is carried out in the framework of the so called multibody context. It consists of considering each component separately from the others but subjected to specific free-body kinematic and loading conditions that are imposed at the connection points of the components.

There are two aerodynamic modelling options in the code: a Blade Element Momentum (BEM) model, which accounts for dynamic inflow, yaw misalignment, and dynamic stall effect and a vortex particle free-wake model. In the present work the BEM option is used. Unsteady aerodynamics associated with TE active shape variations are accounted for by means of FOILFS [20] which has been integrated into the BEM simulation. FOILFS is formulated on the basis of linear airfoil theory that simulates unsteady aerodynamics due to arbitrary camber line variations of a 2D airfoil. The model includes dynamic stall and viscous drag corrections based on the ONERA model. To this end FOILFS requires as input steady-state lift, drag, and moment characteristics of the 2D airfoil section for various flap deployment angles, which in the present analysis have been obtained from FOIL2W [21].

In hGAST the effect of control surfaces on the aerodynamic performance, the structural dynamics of the complete wind turbine and the control system are considered in fully coupled mode. The inertial loads due to TE flap motion are neglected in the present model realization in hGAST since they only have a minor contribution to the blade root moments. It is noted that in the present analyses assessment of the different controllers is performed on the basis of the blade and tower root loads. A detailed design of the full blade with shape morphing capabilities would definitely require taking these loads into account which will be added when the investigation comes to that level of design.

3. Trailing edge shapes

Camber line morphing is performed on the outer part of the blade of the DTU 10 MW turbine. The blade of the reference turbine comprises FFA-w3 series airfoils. The relative thickness of the outer 35% of the blade is constant and equal to t/c=0.24 while further inboards the relative thickness increases to t/c=0.30 at r/R=0.4.

Different morphing shapes of the TE region have been tested. The first configuration (configuration A) corresponds to a short flap that extends to 10% of the chord length. It is based on prior studies performed under Work Package 2 of the UPWIND project for the NREL 5 MW turbine [22]. The camber line deflection shape is defined as a circular arc starting at 90% of the chord length; the radius of the circle is set such that the line connecting the point on the arc at the trailing edge to the flap starting point forms an angle of 1 deg with the un-deformed chord-line. Analytical representation of the deformation shape can be found in [15]. This deformation shape is considered as reference since it has been used in many of the earlier developments on the NREL 5 MW turbine. It is also the reference deflection shape for many of the benchmark exercises comparing different aerodynamic codes (see [20], [22]).

The second family of deformation shapes extends to 30% of the chord length. Longer flaps can be more easily realized by a modular section type. In this case, it is possible to extend the deformable part of the flap to a larger chordwise length and at the same time build the deformation of the camber line more gradually as shown in Figure 1. The articulated shape of the mechanism and the way that the moving parts are arranged, provides greater flexibility than other types of actuators. The morphing mechanism structure consists of pinned moving parts that are designed in a way that can be adjusted and arranged so as the target shape is best followed. Moreover, each part can be activated independently. Thus it is possible to achieve different complex target shapes.

Different morphing shapes (see Figure 2) based on spline curves are assessed in terms of the achieved change in C_L (ΔC_L in Figure 3) for different flap deployment angles. As already mentioned the aerodynamic polars have been computed with FOIL2W at a Reynolds number of 12×10^6, which is

representative over the outer part of the reference blade. Among the various shapes those exhibiting a monotonic behavior (no change of curvature) are qualified and finally the one that provides the maximum ΔC_L (slope 3°) is down selected as configuration B.

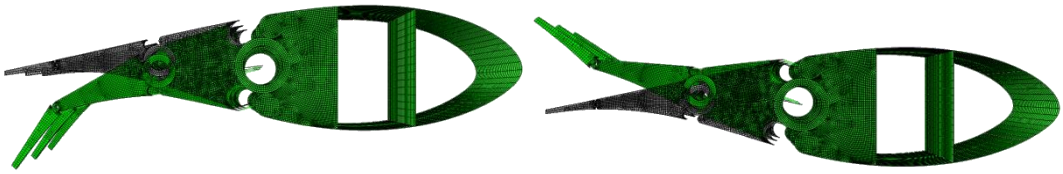

Figure 1. Morphing capabilities by applying a modular flap controlled by SMAs.

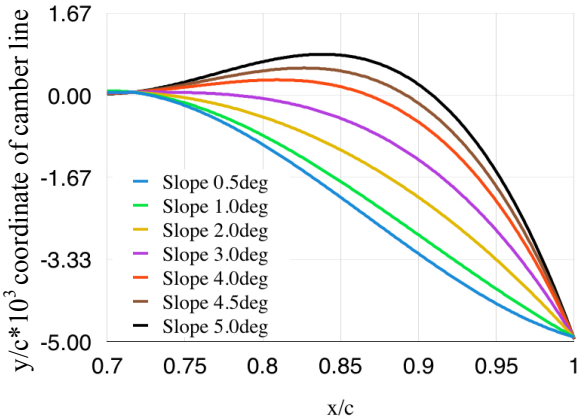

Figure 2. The various Trailing Edge camber line geometries studied.

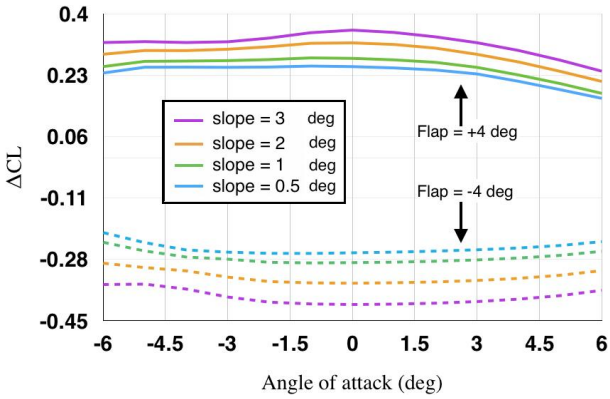

Figure 3. ΔC_L vs. angle of attack for different camber line geometries. Flap angle +/-4 deg.

4. Controller description

The reference turbine is a variable pitch, speed regulated turbine. Individual flap and pitch control have been superimposed to the standard power speed controller of the turbine [9]. A typical individual flap controller (IFC) has been employed [5]. The blade root out-of-plane bending moment signals are transformed into yaw and tilt moments M_{yaw} and M_{tilt} by applying Coleman's transformation. 3p and 6p band-stop filters are applied to M_{yaw} and M_{tilt}. The filtered moments are then passed through and integral control element (I) and the cyclic β_{yaw} and β_{tilt} angles are obtained. These angles are then back transformed into flap angles β_f of the individual blades via an inverse Coleman transformation. The block diagram of the IFC is illustrated in Figure 4. In addition to the IFC, a combined individual pitch-flap controller (IPFC) based on the same working principle is also tested. In the IPFC controller, individual flap control is augmented by simultaneous individual control of the pitch angle of the three blades.

In the present analysis constant controller gains have been used for the individual flap control ($K_{fI} = 5\times10^{-5}$ deg/s/kNm for IFC and $K_{fI} = 7\times10^{-6}$ deg/s/kNm for IPFC). They have been decided based on a sensitivity analysis over a wind speed range of 8-20 m/s. Moreover, it has been observed that the flap control operates efficiently using the same gain values independently of the flap configuration employed. At the current stage of the conceptual design of the system, fine tuning of the controller, including the definition of gain scheduling, was not found necessary, although it is an essential step once the final set up of the flap (dimensions and shape) has been fixed. Constant gains have been also assumed for the individual pitch controller ($K_{PitchI} = 7\times10^{-7}$ deg/s/kNm). In addition, saturation limits have been imposed to the velocity and acceleration of the pitch motion (6 deg/s, 15 deg/s^2). In all configurations a delay of 0.1 s has been imposed to the flap motion in order to

account for the dynamics of the actuator. The general speed limit of the flap motion is set to 100 deg/s (exceptions to the above limit will be discussed in the sequel).

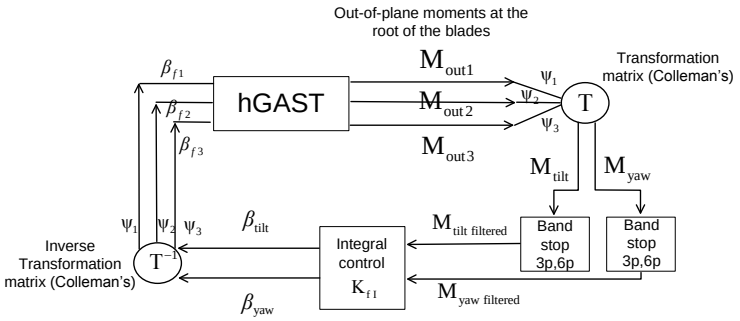

Figure 4. Block diagram of IFC controller.

5. Results and discussion

Four different flap geometries in terms of chordwise and spanwise lengths are investigated. Simulations are performed at the wind speeds of U=8, 12, 14, 16, 20 m/s. For each wind realization a no flap control case (hereafter "no control") has been also simulated. Operation of the flaps in the partial load region is usually not recommended since the interaction of the flap controller with the basic power-speed controller would compromise power production. However, in order to evaluate the above argument, as well as to assess load reduction capabilities at lower wind speeds, the wind speed of U=8 m/s has been also considered (rated wind speed 11.4 m/s). The power production mode is simulated according to DLCs 1.2 and 1.3 of the IEC standard [23]. For each wind speed, six 10min realizations of turbulent wind inflow are performed; both for normal and extreme turbulence conditions (hereafter denoted as "ntm" and "etm" respectively), as defined in the IEC standard for class IA wind turbines. DLC1.2 is a fatigue load case and therefore aims at assessing the fatigue alleviation capabilities of the flap or combined pitch-flap control while DLC 1.3 is considered as the most unfavourable extreme loading situation that effectively determines ultimate design loads. In all cases yaw misalignment and upflow velocity have been set to zero, while the wind shear exponent has been set to 0.2.

Table 1 provides the geometrical characteristics of the configurations studied. "IFC" stands for individual flap control, whereas "IPFC" corresponds to the combined pitch-flap case. Types A, B represent the shape of camber line simulated in accordance with the definitions in section 3. It is noted that a speed limit on the flap motion equal to 100 deg/s has been set to all configurations except configuration 1, which has the smallest size. The reason of letting the speed of configuration 1 unbounded is to enable the assessment of the maximum capabilities of a small flap size even if a much faster actuator would be required. Furthermore, the limit of 100 deg/s is too high for SMAs actuator, although realizable for other types of actuators (e.g. pneumatic). However, as will be shown in the sequel, the above limit was hardly reached by most of the configurations studied in the present work and only at very high wind speeds. Again, the reason for choosing such a relaxed speed limit is that at the present stage, the analysis aims at exploring the maximum potential of the shape morphing concept even in the case a much faster actuator (eg. pneumatic) is to be used.

Table 1. Simulated configurations.

Configuration	Type of camber line	radial position (m)	chord range (m)	flap defl. rate limit (deg/s)
1 (IFC)	A	60-80	3.87-2.34	no limit
2 (IFC)	B	60-80	3.87-2.34	100
3 (IFC)	B	60-85	3.87-1.90	100
4 (IFC)	B	55-85	4.31-1.90	100
Combined (IPFC)	B	60-80	3.87-2.34	100

The resulting fatigue loads are assessed in terms of the 1 Hz Equivalent Fatigue Damage Load (DEL) reduction achieved by the different configurations in comparison to the "no control" case. For calculating the DELs, exponent values of m=10 and m=4 were used for the blades and the tower loads respectively. The DEL considered for each wind speed is the average of the DELs of all six realizations and of the three blades. The impact on the extreme blade loads is assessed through the comparison of the ultimate flapwise moments. The maximum/minimum load amongst all realizations and all three blades is considered as ultimate load. Loads are computed at the root of the blade and at the base of the tower.

In the sequel, the assessment of the various configurations in terms of load reduction potential is first presented. Then, control motion characteristics of the different configurations are shown. Finally, the influence of each configuration on power production is assessed.

Figure 5 and Figure 6 present the results of the fatigue loads reduction for "ntm" and "etm" conditions respectively. Although "etm" is defined by the standards as an ultimate DLC, the assessment of the fatigue loads reduction capabilities of the control system for increased turbulence values was considered to be an interesting exercise. Results are presented for all simulated wind speeds and configurations as normalized equivalent load values with respect to the corresponding values of the "no control" case.

All configurations alleviate significantly the fatigue loads experienced by the blades. Overall, the reduction is smaller at extreme turbulence conditions at all wind speeds which indicates that the configurations considered reach their limits as the turbulence levels increase. The benefit of a longer flap is evident as the wind speed increases. For the "ntm" case at U=8 m/s all configurations achieve a similar level of reduction which is around 10%. That is because the loads at this wind speed are still moderate and all flap configurations achieve the target of zeroing the mean of M_{yaw} and M_{tilt} (target set by the controller - equivalent to minimizing the amplitude of the 1p variation in the rotating frame). Therefore, in the partial load region all configurations appear to have a similar performance. At U=12 m/s (just above the rated wind speed) the difference in the efficiency of the different configurations becomes more evident. Configuration 1 cannot reduce the fatigue load more than what achieved at 8 m/s while configurations 2-4 reduce the loads by an additional 6%-8%. As the wind speed increases, the longer flaps yield higher fatigue load reduction. Furthermore, the combined pitch-flap control behaves in a similar manner as the longer flaps (configurations 3 and 4). The performance of IPFC clearly increases as the wind speed increases. It is also noted that overall, the combined control achieves the highest reduction rates ranging between 11% (at low wind speeds) to 27% (at high wind speeds).

Similar trends are obtained for the "etm" cases. Configuration 1 provides a marginal reduction in the loads, which varies between 3% to a maximum value of 6%. As the size of the flap increases, higher reduction rates are achieved which are however smaller than those in "ntm" conditions. Also, the difference in the load reduction of the longer flaps (radial extent greater than 20 m), as compared to the shorter ones, increases with the wind speed. As in the "ntm" case the combined control provides the highest reductions rates: 9% to 24%.

The standard deviation (sdv) plots of the M_{yaw} and M_{tilt} moments as functions of the wind speed shown in Figure 7 and Figure 8, substantiate the above remarks. Given that the controller aims at zeroing out the yaw and tilt moments, a reduction of their sdv indicates reduction of blade flapwise loads. It is seen that as the size of the flaps increases the sdv of the above moments decreases. The greater reduction of the sdv is obtained with the combined pitch - flap control. It is evident in this case that individual pitch control augments the flap in zeroing the tilt and yaw moments.

Figure 9 and Figure 10 show the results of the edgewise moment for "ntm" and "etm" respectively in terms of the 1 Hz DELs. It is seen that none of the configurations - either in "ntm" or "etm" - substantially affects the equivalent loads in the edgewise direction. This is expected as the edgewise moment is mainly driven by gravitational loads. Marginal reduction or increase in the edgewise loads of the order of 2% is noted depending on the wind velocity.

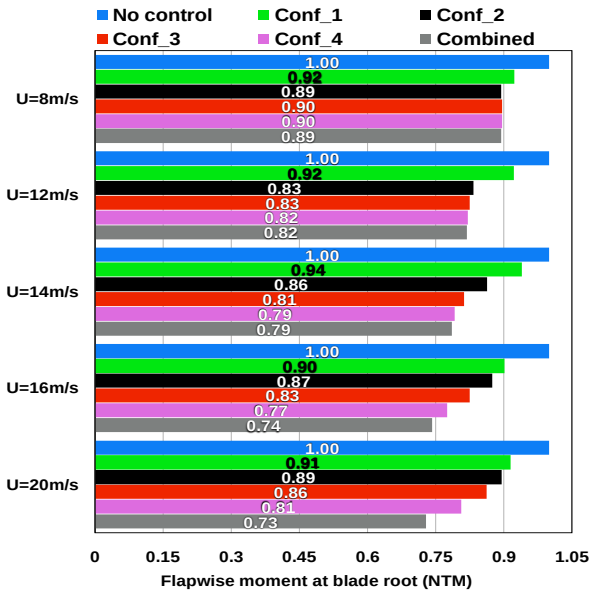

Figure 5. Normalized DELs (m=10) of blade root flapwise moment (ntm).

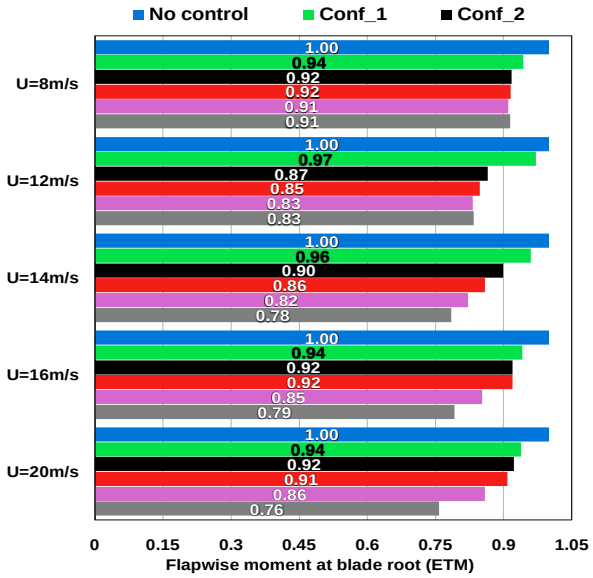

Figure 6. Normalized DELs (m=10) of blade root flapwise moment (etm).

Figure 11 and Figure 12 present the results of the fore-aft equivalent moment, at the base of the tower, in "ntm" and "etm" conditions. The general pattern in both cases is independent of the flap configuration. Up to the rated wind speed, the flap control does not affect the tower fore-aft loads. Beyond 14 m/s a slight increase of the equivalent load is observed that is of the same order for both turbulent inflow conditions (1% to 6%). A marginal increase in the tower fore-aft loads of 1% -3% is obtained with the combined flap-pitch controller.

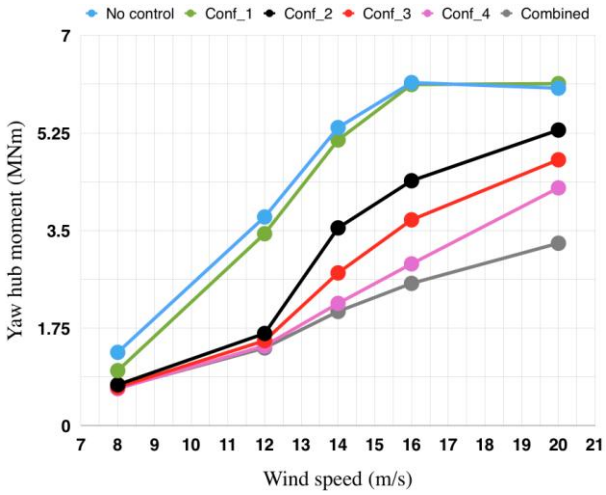

Figure 7. Sdv of M_{yaw} for one specific realization at "ntm".

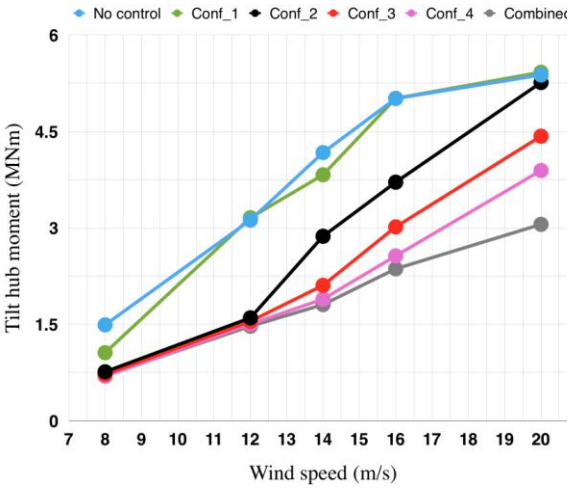

Figure 8. Sdv of M_{tilt} for one specific realization at "ntm".

Figure 13 and Figure 14 show the results of the equivalent side-side moment at the bottom of the tower for the two turbulent conditions. In the "ntm" case, a reduction of approximately 3% to 5% is achieved up to the wind speed of 12 m/s. This is not directly related to the size of the flap (for example at U=12 m/s configuration 3 provides a higher reduction than configuration 4). As in the case of the fore-aft tower moment an increase in the loads is observed for wind speeds higher than 14 m/s of the order of 1%-5%. The picture totally changes in "etm" conditions. At 8m/s all configurations significantly increase the side-side moment (the combined pitch-flap controller included). Again no

relation to the length of the flap is noted. As the wind speed increases lower increase rates are obtained, slightly higher than those seen in "ntm" conditions.

In Figure 15 the effect of the flaps on the extreme flapwise moment at the root of the blade in "etm" conditions is depicted. Table 2 contains the percentage variation of the maximum and minimum extreme loads with respect to the "no control" case. Although none of the configurations reduces the maximum/minimum blade flapwise loads at all wind speeds, the ultimate loads are reduced by all configurations. Higher reduction rates are obtained for the minimum loads. Marginal reduction of the maximum flapwise moment (up to about 4% for the longest flap size) is obtained for the flap control while a much higher reduction of about 9% is obtained for the combined pitch-flap control. The reduction of the minima ranges between 5%-30%. The highest reduction is again obtained with the combined pitch-flap controller. It is noted that the individual flap controller has not been specifically designed for reducing extreme loads.

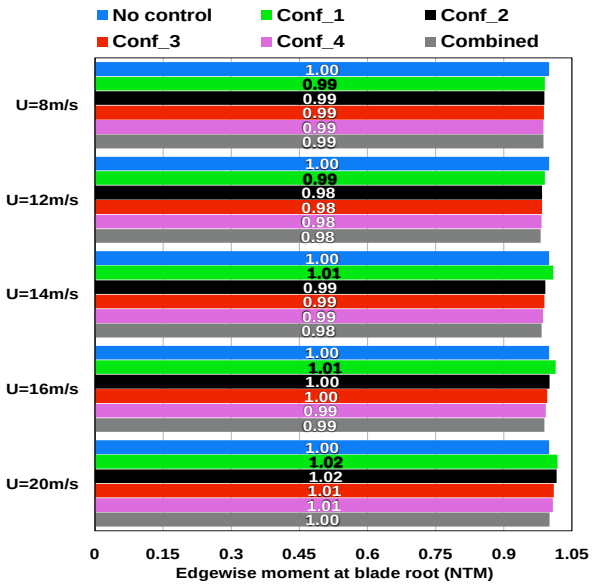

Figure 9. Normalized DELs (m=10) of blade root edgewise moment (ntm).

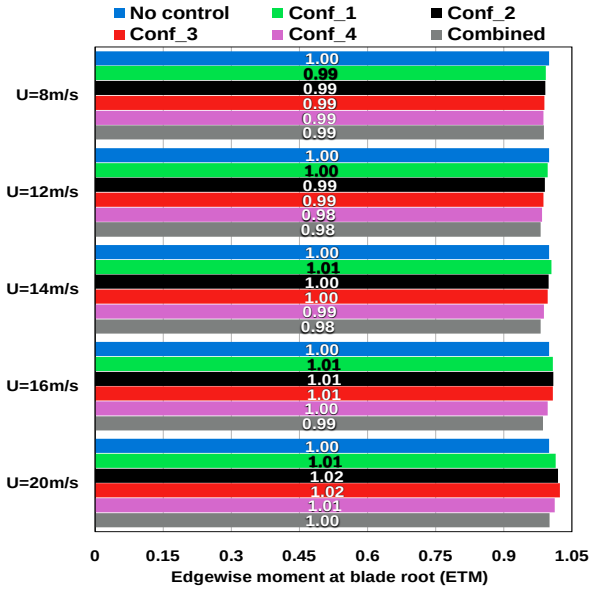

Figure 10. Normalized DELs (m=10) of blade root edgewise moment (etm).

As detailed in section 4 the aim of the IFC controller is to mitigate the 1p variation of the flapwise loads. As a spin off, peaks of the flapwise moment are also truncated. However, there are cases where in the occurrence of a gust, the controller fails to respond quickly enough and to filter the peak load. So the maximum/minimum load increases. The above is explained through a time series example of the flapwise moment shown in Figure 16. In this figure the time series of the flapwise moment for the "no control" case is compared against the time series of configurations 2 and 4 at U=16 m/s. As shown earlier this is a case where configuration 2 increases the maximum flapwise moment. In the same plot the time series of the hub velocity is also presented together with the flap angle time series of the two configurations. The ultimate (maximum) load occurs shortly before t=380 s. The increase in the flapwise moment is a consequence of the rapid increase in wind velocity from about 5 m/s to 15 m/s within 10 s. As seen in Figure 16 configuration 2 fails to truncate the maximum loads while some reduction is achieved by the longer flap (configuration 4). The flap angle plot indicates that shortly before the gust occurs, configuration 2 has reached the maximum flap deflection of 10 deg. When the gust occurs the flapwise moment increases while the flap angle is stuck to the positive bound of +10 deg. On the contrary in configuration 4 the flap angle moves fast in the opposite direction (towards negative angles) and therefore flap control manages to cut-off the overshoot in the flapwise bending moment. The rapid increase in wind velocity results in a sudden increase of the yaw moment, the zeroing of which requires a change in the sign of β_{yaw}. When the sign of β_{yaw} changes a 180 deg

phase shift in the response of the blade flap angle β_f takes place. This eventually leads to motion of the flap towards negative angles. In configuration 2 the controller fails to change quickly enough the sign of β_{yaw} and therefore the flap angle β_f of the blade remains stuck at its positive upper bound. For the same wind speed the IPFC configuration reduces the ultimate flapwise moment (see Figure 15) although it employs the same flap geometry as configuration 2. This is due to the contribution of the individual pitch control action which effectively controls the yaw and tilt moments of the rotor.

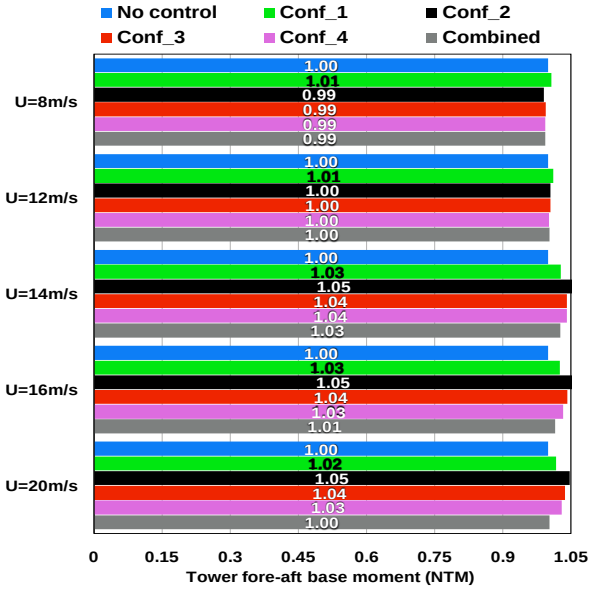

Figure 11. Normalized DELs (m=4) of tower bottom fore-aft moment (ntm).

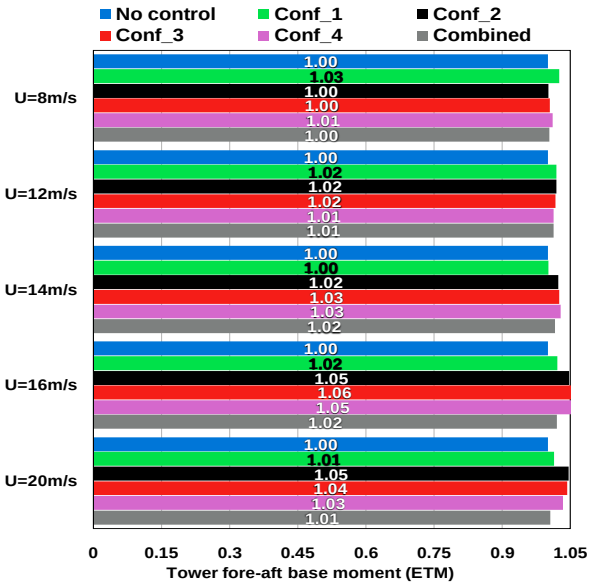

Figure 12. Normalized DELs (m=4) of tower bottom fore-aft moment (etm).

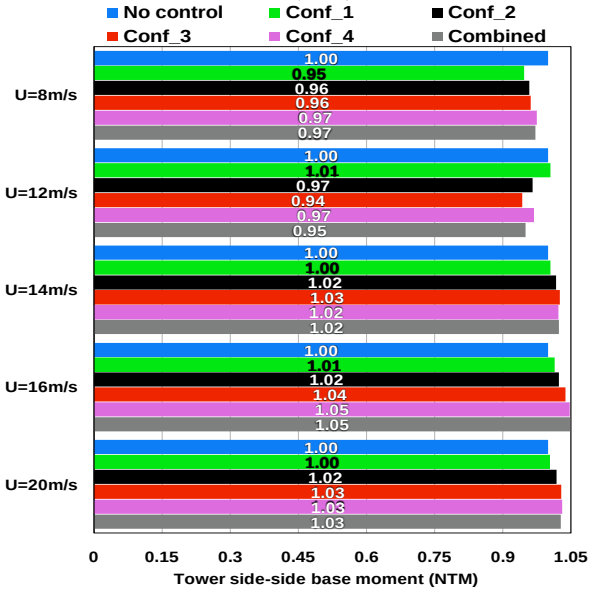

Figure 13. Normalized DELs (m=4) of tower bottom side-side moment (ntm).

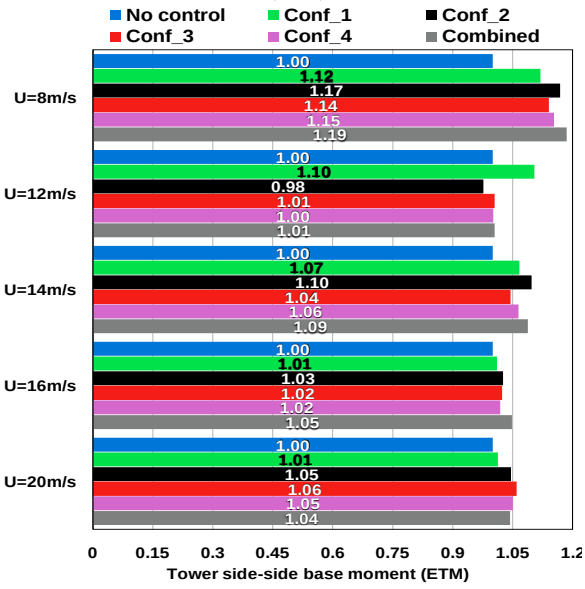

Figure 14. Normalized DELs (m=4) of tower bottom side-side moment (etm).

In Figure 17 and Figure 18 the statistics (maximum, minimum, standard deviation) of the flap motion (average values of six realizations), for all configurations and wind speeds and for both turbulence conditions are shown. As the size of the flap increases a reduction in the extreme flap angle is observed at below rated wind speeds. In the full load region all configurations reach the saturation limits of +/-10 deg. In the "ntm" case the smaller flap (configuration 1) reaches the saturation limit

already at 8m/s wind speed. At the same wind speed the peak angle of configuration 4 (largest flap) is about half of its limit. It is also seen that when a small flap is augmented by individual pitch control (combined control), the peak flap angle is almost at the same level as with a much longer flap (configuration 4) and no pitch control. The sdv of the flap angle shows that less flap actuation is required as the size of the flap increases, either in the chordwise or in the spanwise direction. A substantial reduction of the sdv is obtained when increasing the chordwise length of the flap, especially at lower wind speeds (see configuration 1 against 2). On the other hand, the increase of the size of the flap in the spanwise direction leads to a further reduction of the sdv which appears to be almost independent of the wind speed (note the almost constant difference among the sdvs of all the IFC cases independent of the wind velocity). An exception to the above remark is the case of 8 m/s where no reduction on the sdv of the flap motion is noted as the spanwise length of the flap increases. Combined pitch - flap configuration results in the lowest values of the sdv especially at high wind speeds.

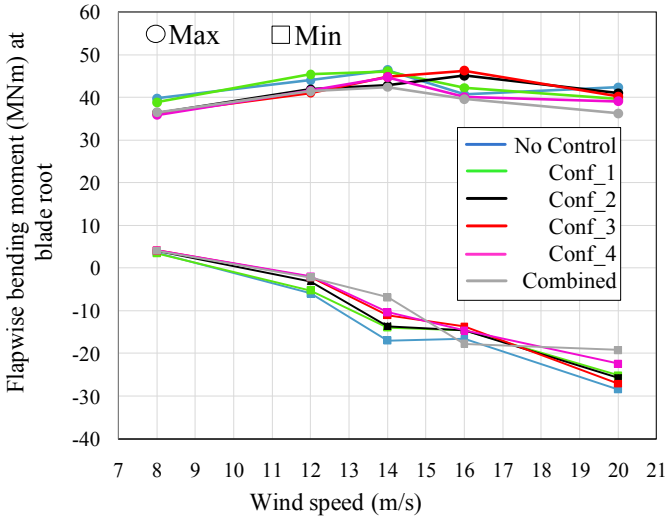

Figure 15. Maximum and minimum of flapwise moment at blade root (etm). Safety factors not applied.

Table 2. Statistics of Figure 15.

Configuration	*Variation of max (%)*	*Variation of min (%)*
1	**-0.7**	**-11.6**
2	**-2.9**	**-9.6**
3	**-0.3**	**-5.0**
4	**-3.6**	**-21.4**
combined	**-8.7**	**-32.5**

Similar trends are observed under “etm” conditions. It is noted that the sdv of the flap motion is not considerably affected by the level of turbulence. Moreover, the fact that none of the configurations but the smallest one (configuration 1) reaches the saturation limits at the wind speed of 8 m/s (independently of the turbulence model), indicates that higher gains could have been used at below rated wind speeds for higher load reduction levels.

The maximum absolute value of the flap velocity (peak value of time series for all wind seeds) for all configurations and wind velocities and for both turbulent conditions is presented in Figure 19 and Figure 20. It is seen that the unbounded configuration 1 gives unrealistically high flap velocities as the wind speed increases (the limit of 100 deg/s set for the other configurations is being exceeded by far). So, for the smallest flap configuration, not only the reduction of the loads is marginal but it can be only achieved with very high velocities of the flap motion. In this case, the flap moves fast between the upper and lower bounds (+/-10 deg) in an effort to achieve the maximum possible reduction of the sdv of M_{yaw} and M_{tilt}. A small increase of the chordwise extent of the flap results in substantially smaller peak velocities (e.g. the bound velocity is hardly reached under “ntm” conditions). Additional but smaller reduction of the flap velocity is obtained when increasing the spanwise extent of the flap. The combined pitch-flap control provides the lowest flap velocities. An almost linear increase in the flap velocity with the wind speed is observed in “ntm” conditions that ranges from 5 deg/s-27 deg/s while in “etm” conditions the flap velocities range from 8 deg/s-42 deg/s. As expected maximum flap velocities increase as we move from “ntm” to “etm” conditions at all wind speeds and independent of the flap configuration employed. As the wind speed increases, the contribution of the individual pitch

control to load alleviation gets higher and therefore speed requirements for the flap motion are relaxed. The difference in the maximum flap velocity between the IFC and the IPFC cases becomes distinct for wind velocities higher than 14 m/s.

It is noted that for IFC and IPFC, the flap signal follows in general a variation with 1p frequency (as shown in Figure 16). As a result, most of the time the flap speed is not exceeding 10 deg/s (maximum rotor speed equals ~1 rad/s). A higher flap speed (exceeding 10 deg/s or the bound of 100 deg/s) is only reached when the flap angle reaches the saturation limit of +/-10 deg. For the IPFC controller, or for bigger flaps (Configuration 2-4), this may happen only few times within the 10 minutes of the simulation. In this case of course an SMA actuator will not be able to follow however this is not expected to compromise the overall load reduction capabilities of the system.

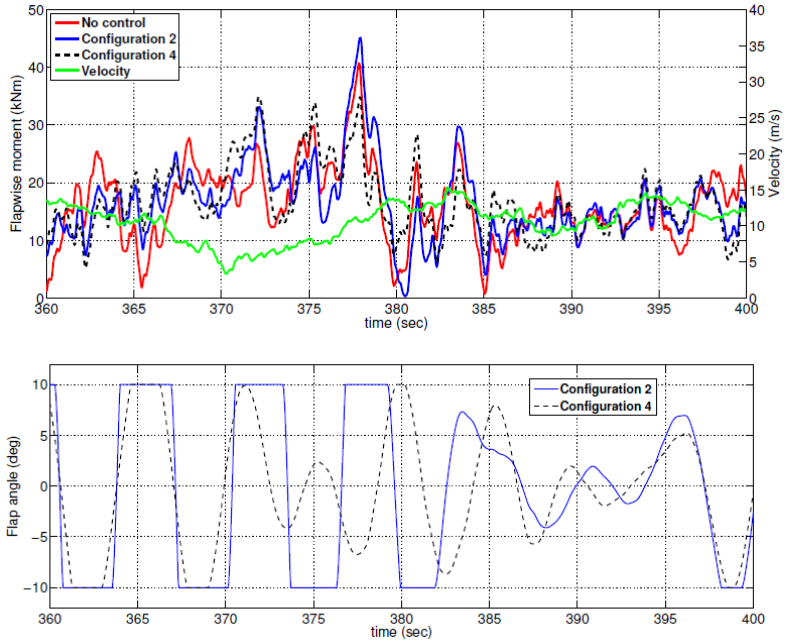

Figure 16. Time series of flapwise bending moment at blade root and flap angle. Comparison of Configuration 2 and 4 at 16 m/s for “etm”.

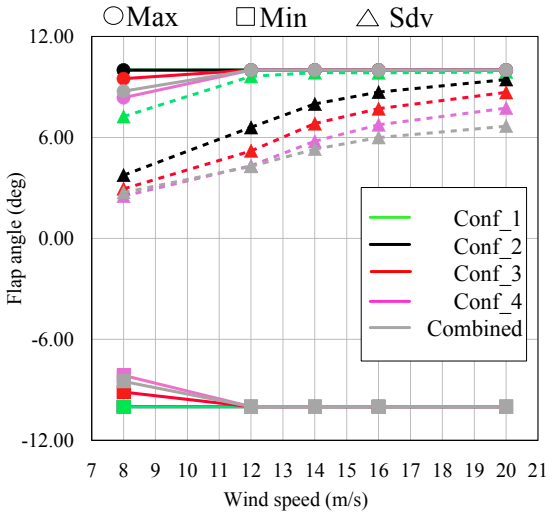

Figure 17. Maximum, minimum and standard deviation of the flap movement (ntm).

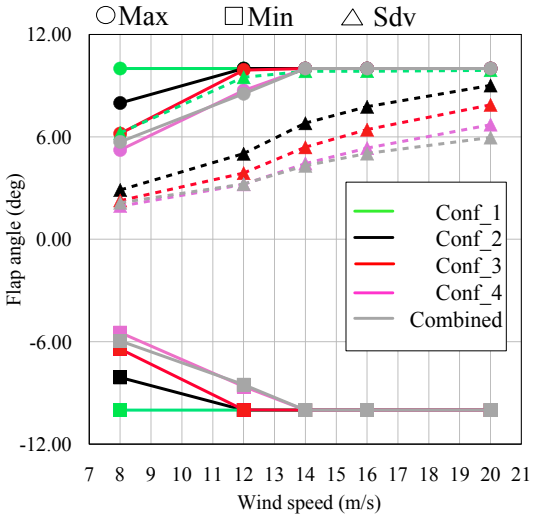

Figure 18. Maximum, minimum and standard deviation of the flap movement (etm).

Undesired interactions between the IFC and the standard pitch controller used for power regulation are assessed through analyzing power output results. The average sdv of the pitch motion (for wind speeds in the full load region) and the average of the mean power (for all wind speeds) of all realizations are calculated for both turbulent conditions. The results of the pitch angle sdv are summarized in Table 3 while the results of the mean power are presented in Table 4. For the "ntm" case, in the full load region, the effect of IFC on power output is almost negligible and compensated by the pitch controller. It is seen that for wind speeds above 14 m/s, the pitch activity increases for all IFC configurations. The highest increase of about 6%-7% is noted at the wind speed of 14 m/s and for the bigger flap sizes. At higher wind speeds the sdv increases by 2% at most. At the wind speed of 12 m/s pitch activity decreases for all flap configurations. As a result a mean power reduction of 1% is recorded. It is noted that the wind speed of 12 m/s is slightly above the rated velocity. Therefore, at this wind speed the controller continuously switches between variable speed and variable pitch modes of operation. Thus, in case where the flap control results in reduced rotor speed, pitch regulation is unable to drop below its lower limit of 0 deg angle and therefore it cannot compensate the consequent power loss. A more dedicated design of the transition operation of the controller would probably recover this power loss. At 8m/s wind speed an appreciable power loss of about 2% is obtained with all configurations which justifies the choice of lower gains although this would limit the fatigue reduction. In "etm" conditions a reduction of the mean power output is observed in the wind speed range of 8 m/s-14 m/s. The highest reduction rate (up to 3%) is noted at the wind speed of 8 m/s. At wind speeds of 12 m/s and 14 m/s, the mean power losses go up to 2% and 0.6% respectively. Again the bigger the size of the flap is, the loss of power becomes higher. Due to the higher turbulence level the previously reported inability of the pitch controller to compensate power losses when pitch angle drops down to 0 deg is now extended up to the wind velocity of 14 m/s.

The mean power loss of the IPFC configuration is slightly lower than that of the IFC configurations with bigger flap sizes which provide higher load reduction levels. At moderate wind speeds up to 14 m/s the increase of the pitch activity of the IPFC is negligible while at high wind speeds the reduction of the sdv of the flap motion comes at an expense of an increased pitch activity which is now 5% -7% higher than that of the no flap control case.

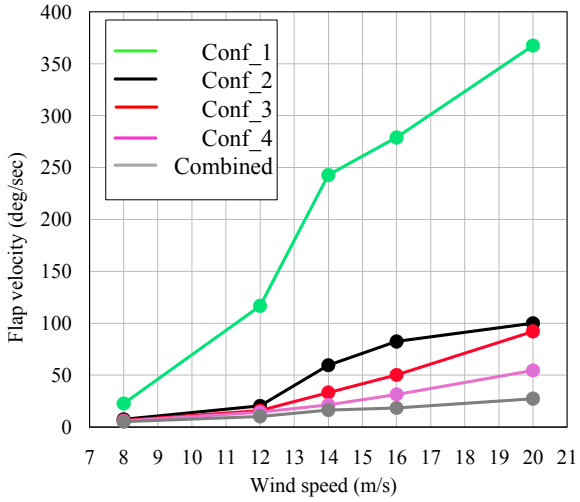

Figure 19. Maximum absolute values of flap velocity (ntm).

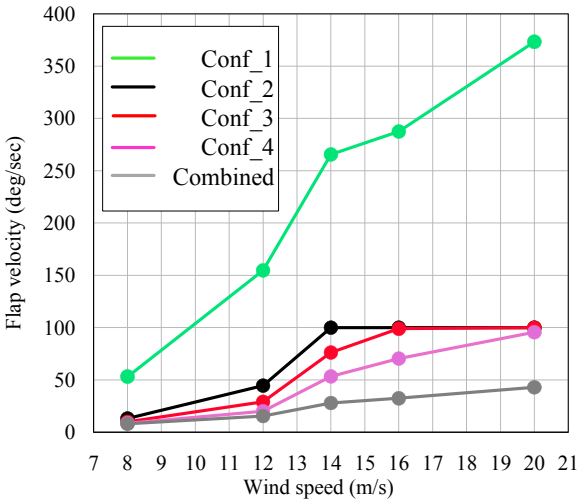

Figure 20. Maximum absolute values of flap velocity (etm).

Table 3. Percentage change of the pitch sdv with respect to the "no control" case. Wind speeds in full load conditions (a) ntm, (b) etm.

Wind speed (m/s)	$Conf_1$	$Conf_2$	$Conf_3$	$Conf_4$	$Combined$
12	-0.4	-0.34	-0.17	-0.01	0.54
14	3.2	7.3	6.5	6.4	7.3
16	1.3	2.7	2.6	2.2	5.2
20	0.5	1.6	0.9	1.0	6.8

(a)

Wind speed (m/s)	$Conf_1$	$Conf_2$	$Conf_3$	$Conf_4$	$Combined$
12	-0.51	-1.2	-0.87	-0.85	-0.052
14	1.1	2.0	2.2	2.8	3.9
16	1.6	4.0	4.4	5.1	7.5
20	0.52	1.8	1.8	1.5	7.2

(b)

Table 4. Percentage change of the mean power (a) ntm, (b) etm.

Wind speed (m/s)	$Conf_1$	$Conf_2$	$Conf_3$	$Conf_4$	$Combined$
8	-1.70	-1.84	-1.84	-2.00	-1.78
12	-0.64	-0.92	-0.89	-0.93	-0.82
14	0.07	0.08	0.01	0.03	0.10
16	0.10	0.14	0.04	0.06	0.16
20	0.14	0.24	0.10	0.13	0.30

(a)

Wind speed (m/s)	$Conf_1$	$Conf_2$	$Conf_3$	$Conf_4$	$Combined$
8	-2.08	-2.87	-2.83	-3.21	-2.83
12	-0.92	-2.01	-1.90	-1.99	-1.79
14	-0.16	-0.56	-0.62	-0.59	-0.44
16	0.10	0.12	-0.02	0.00	0.14
20	0.13	0.24	0.04	0.08	0.30

(b)

6. Conclusions

Fatigue load reduction capabilities of IFC and IPFC are assessed on a 10 MW turbine. Different camber line geometries as well as flaps of different chordwise and spanwise dimensions are evaluated. Blade flapwise fatigue load reduction of about 6-10% is attained with IFC using a flap of 10% chordwise and 20% spanwise length. Earlier developments on the NREL 5 MW turbine suggested that a flap having the above dimensions can achieve 15-20% reduction of the flapwise load. This indicates that as the rotor diameter increases the requirements set to IFC controller become more demanding. Higher reduction of about 20% is obtained with a flap of 30% chordwise and 30% spanwise extent. Flapwise fatigue load reduction of about the same order is obtained for IPFC but with a shorter flap extending to 20% of the span. Overall, a slight increase not exceeding 6% is obtained in the tower bottom loads (both in fore-aft and side-to-side direction) for all configurations considered. Although the controllers are not designed to reduce ultimate loads a small reduction of the ultimate flapwise moment is achieved with all configurations with the IPFC exhibiting best performance. A minor effect on power output is noted especially at wind speeds in the full load region. Finally, maximum flap motion velocities recorded with IPFC that do not exceed 27 deg/s in "ntm" indicate that such a controller is possible to be combined with SMA type actuators.

7. Acknowledgments
The work presented in paper was partially funded from the European Community's Seventh Framework Program under grant agreement No. FP7-ENERGY-2012-1-2STAGE-308974 (INNWIND.EU)

References
[1] Karakalas, A., Machairas, T., Solomou, A., Riziotis, V., Saravanos, D. 2014, Design and Simulation of Morphing Airfoil Sections with SMA Actuators for Wind Turbine Rotors. ICAST2014: 25nd International Conference on Adaptive Structures and Technologies, October 6-8th, The Hague, The Netherlands, ICAST2014 082.
[2] Karakalas, A., Machairas, T., Solomou, A., Riziotis, V., Saravanos, D., 2015, Morphing Airfoil with Shape Memory Alloy Wire Actuators for Active Aerodynamic Load Control in Large Wind-Turbine Blades, *EWEA annual event*, 17-20 November, Paris.
[3] Bossanyi, E.A., 2003, Wind Turbine Control for Load Reduction, *Wind Energy, 2003, 6, 229-244.*
[4] Lackner MA, van Kuik G., 2010, A comparison of smart rotor control approaches using trailing edge flaps and individual pitch control, *Wind Energy 2010;13:117–34*.
[5] Bæk P., 2011, Unsteady Flow Modeling and Experimental Verification of Active Flow Control Concepts for Wind Turbine Blades, DTU RISOE, 2011. PhD Thesis.
[6] Bernhammer, L., van Kuik G., De Breuker, R., 2016, Fatigue and Extreme Load Reduction of Wind Turbine Components using Smart Rotors, *J. WindEng.Ind.Aerodyn.154,84–95*.
[7] Barlas, T.K., van der Veen, G., van Kuik G., 2012, Model predictive control for wind turbines with distributed active flaps: incorporating inflow signals and actuator constraints, *Wind Energy 15(5):757–71*.
[8] Bergami, L., Poulsen, N., 2014, A smart rotor configuration with linear quadratic control of adaptive trailing edge flaps for active load alleviation, *Published online in Wind Energy*.
[9] Bak, C., Zahle, F., Bitsche, R., Kim, T., Yde, A., Henriksen, L.C., Natarajan, A., Hansen, M.H., 2013, Description of the DTU 10 MW Reference Wind Turbine, DTU Wind Energy Report-I-0092.
[10] Riziotis, V.A., Madsen, H.A., Rasmussen, F., Politis, E.S., Voutsinas, S.G., 2012, Implications on loads by up-scaling towards 20MW size, *EWEA Annual Event*, 16-19 April, Copenhagen.
[11] Solomou Alexandros, Machairas Theodoros, Saravanos Dimitrios, 2014, A coupled thermomechanical beam finite element for the simulation of shape memory alloy actuators, *Journal of Intelligent Materials Systems and Structures*, 25, 890-907.
[12] Solomou Alexandros, Machairas Theodoros, Saravanos Dimitrios, Hartl Darren, Lagoudas Dimitrios, 2016, A coupled layer thermomechanical shape memory alloy beam element with enhanced higher order temperature field approximations, *Journal of Intelligent Materials Systems and Structures*, in press.
[13] Hartl Darren, Lagoudas Dimitris, 2007, Aerospace Applications of Shape Memory Alloys, *Proceedings of Mechanical Engineers, Journal of Aerospace Engineering, Part G*, Volume 221, No.4, pp. 535-552.
[14] A. W. Hulskamp, H. Champliaud, H. E. N. Bersee, 2009, Design and Analysis of a Scaled Smart Rotor Blade for Wind Turbine Load Control, *17th International Conference on Composite Materials*, Edinburgh, Scotland, UK.
[15] S. Barbarino, R. Pecora, L. Lecce, A. Concilio, S. Ameduri, E. Calvi, 2009, A Novel SMA-based Concept for Airfoil Structural Morphing, *Journal of Materials Engineering and Performance*, Volume 18, Issue 5, pp. 696-705.
[16] A. Lara-Quintanilla, H. E. N. Bersee, 2013, A Study on the Contraction and Cooling Times of Actively Cooled Shape Memory Alloy Wires, *Journal of Intelligent Material Systems and Structures*, Volume 27, Number 03, pp. 403-417.
[17] Riziotis, V. A. , Voutsinas, S. G., 1997, Gast: A General Aerodynamic and Structural Prediction Tool for Wind Turbines, *Proceedings of the EWEC'97*, Dublin, Ireland.

[18] Manolas D.I., Riziotis, V.A., Voutsinas, S.G, 2015, Assessing the importance of geometric non-linear effects in the prediction of wind turbine blade loads, *Computational and Nonlinear Dynamics Journal*, Vol. 10, 041008, July 2015.
[19] Popko, W., Vorpahl, F., Zuga, A., Kohlmeier, M., Jonkman, J., Robertson, A., Larsen, T.J., Yde, A., Sætertrø, K., Okstad, K.M., et al, 2014, Offshore Code Comparison Collaboration Continuation (OC4), Phase I—Results of Coupled Simulations of an Offshore Wind Turbine with Jacket Support Structure. *Journal of Ocean and Wind Energy*, 1(1): p. 1-11.
[20] Barlas,T., Jost, E., Pirrung, G., Tsiantas,T., Riziotis,V., Navalkar, S.T., Lutz,T., van Wingerden, J.W.,2016, Benchmarking aerodynamic prediction of unsteady rotor aerodynamics of active flaps on wind turbine blades using ranging fidelity tools, *To be presented in the Science of Making Torque from the Wind Conference*, TUM Munich, Germany, October 5-7.
[21] Riziotis, V.A., Voutsinas, S.G., 2008, Dynamic stall modeling on airfoils based on strong viscous-inviscid interaction coupling, *J. Numerical Methods in Fluids*, 56, pp 185-208.
[22] Bergami L, Riziotis V, Gaunaa M. , 2014, Aerodynamic response of an airfoil section undergoing pitch motion and trailing edge flap deflection: a comparison of simulation methods, *published online on Wind Energy*.
[23] IEC. IEC 61400-1. 2005, Wind turbines – Part 1: Design Requirements.